

Incommensurate antiferromagnetic order in weakly frustrated two-dimensional van der Waals insulator CrPSe₃

Baithi Mallesh^{1,2}, Ngoc Toan Dang^{3,4,*}, Tuan Anh Tran⁵, Dinh Hoa Luong^{1,2}, Krishna P. Dhakal², Duhee Yoon¹, Anton V. Rutkauskas⁶, Sergei E. Kichanov⁶, Ivan Y. Zel⁶, Jeongyoung Kim², Denis P. Kozlenko^{6,*}, Young Hee Lee^{1,2,7,*}, Dinh Loc Duong^{1,2,*}

¹Center for Integrated Nanostructure Physics, Institute for Basic Science, Suwon 16419, Republic of Korea

²Department of Energy Science, Sungkyunkwan University, Suwon 16419, Republic of Korea

³Institute of Research and Development, Duy Tan University, 550000 Danang, Vietnam

⁴Faculty of Environmental and Natural Sciences, Duy Tan University, 550000 Danang, Vietnam

⁵Ho Chi Minh City University of Technology and Education, 700000 Ho Chi Minh, Vietnam

⁶Frank Laboratory of Neutron Physics, Joint Institute for Nuclear Research, 141980 Dubna, Russia

⁷Department of Physics, Sungkyunkwan University, Suwon 16419, Republic of Korea

*Correspondence to: dangngoctoan1@duytan.edu.vn, denk@nf.jinr.ru, leeyoung@skku.edu,

l.duong1902@gmail.com

Abstract

Although the magnetic order is suppressed by a strong magnetic frustration, it is maintained but appears in complex order forms such as a cycloid or spin density wave in weakly frustrated systems. Herein, we report a weakly magnetic-frustrated two-dimensional van der Waals material CrPSe₃. Polycrystalline CrPSe₃ was synthesized at an optimized temperature of 700 °C to avoid the formation of any secondary phases (e.g., Cr₂Se₃). The antiferromagnetic transition appeared at $T_N \sim 126$ K with a large Curie–Weiss temperature $\theta_{CW} \sim -371$ K via magnetic susceptibility measurements, indicating weak frustration in CrPSe₃ with a frustration factor $f (|\theta_{CW}/T_N) \sim 3$. Evidently, the formation of long-range incommensurate spin-density wave antiferromagnetic order with the propagation vector $\mathbf{k} = (0, 0.40, 0)$ was revealed by neutron diffraction measurements at low temperatures (below 120 K). The monoclinic crystal structure of C2/m symmetry is preserved over the studied temperature range down to 20 K, as confirmed by Raman spectroscopy measurements. Our findings on the spin density wave antiferromagnetic order in two-dimensional (2D) magnetic materials, not previously observed in the MPX₃ family, are expected to enrich the physics of magnetism at the 2D limit, thereby opening opportunities for their practical applications in spintronics and quantum devices.

I. INTRODUCTION

Two-dimensional (2D) van der Waals (vdW) magnetic materials are increasingly being recognized for their potential application in next-generation spintronic devices [1–5]. These materials in atomically thin forms give rise to controlling magnetic order and physical properties by gate bias, strain, and proximity effects [3–10]. To explore novel materials and the physics of magnetism at the 2D limit, both intrinsic-magnetic and magnetic-doped 2D vdW materials have been synthesized and investigated [5,11–19]. Whereas the latter class requires sophisticated efforts in designing and investigation, the exploration of intrinsic 2D vdW magnetic materials relies on the available bulk forms like ferromagnetic insulating CrBr_3 [20] and CrI_3 [16], semiconducting CrGeTe_3 [15], metallic Fe_3GeTe_2 [21], and antiferromagnetic insulating MPX_3 ($M = \text{Fe}, \text{Mn}, \text{Ni}$, $X = \text{S}, \text{Se}$) systems [14,22–24]. In the most of these materials, the long-range magnetic order is retained in atomically thin forms, and in some cases like CrI_3 , the inter layer magnetic interactions can be tuned from FM to AFM by mediating the layers number [16]. Furthermore, the antiferromagnetic order in MPX_3 can assist in the formation of coherent excitons [25,26], indicating an appropriate family of materials to investigate the Bose-Einstein condensation of excitons [26]. These materials are also suitable prototypes to search for high- T_C superconductors by doping or using pressure [27].

Another important feature of the MPX_3 vdW materials is a diversity of commensurate antiferromagnetic orders, realized on structurally similar lattices with a hexagonal-like arrangement of transition metal atoms in the vdW layers (Table I). The magnetic structures can be Néel or zigzag with Heisenberg (MnPS_3 [28–31]), XY (NiPS_3 [32–35]), and Ising (FePS_3 [28,31,35–38]) types, which depend solely on the exchange coupling energies between transition metal ions in the lattice. The magnetic structures and magnetic ordering temperatures

are mediated by the strength and correlation between the first-, second-, and third-neighbor interactions of the in-plane metal atoms [28,29]. The interlayer exchange coupling, though relatively weak, plays a crucial role in the formation of the magnetic order along the c axis [34].

Although the MPX_3 family has diverse magnetic properties, none of the explored MPX_3 materials exhibit spin frustration or incommensurate spin arrangements. In this report, for the first time, we explore a weak spin frustration system in this family, $CrPSe_3$. It crystallizes in the monoclinic structure of $C2/m$ symmetry and orders antiferromagnetically at the Néel temperature $T_N \sim 126$ K. The large frustration factor, $f = |\theta_{CW}/T_N$ (~ 3) implies that $CrPSe_3$ has weak spin-frustration. The modulated spin density wave and incommensurate AFM order in $CrPSe_3$, revealed by neutron diffraction experiments, bring novel prospects for further search of related compounds for studies of magnetic frustration effects and their interplay with physical properties of the layered 2D vdW compounds.

II. EXPERIMENTAL PROCEDURE

As the first stage of synthesis procedure, a polycrystalline powder of $CrPSe_3$ was synthesized by a solid-state reaction. Reagents of Cr (powder, 200 mesh, Alfa Aesar, 99.99%), P (red, lumps, Alfa Aesar, 99.99%), and Se (crushed granules, Alfa Aesar, 99.999%) were ground together under ambient conditions. Approximately 2 g of materials with their stoichiometric ratio $Cr:P:Se = 1:1:3$ were pressed as a pellet at 0.1 MPa pressure, followed by sealing in a quartz ampule ($22 \times 25 \times 100$ mm) under high vacuum ($< 5 \times 10^{-3}$ Torr). The sealed ampule was kept in a box furnace at 700 °C with a ramp rate of 1.6 °C per min for a 10-day holding time, followed by furnace cooling. At the second stage, the single crystals were prepared using this powder. This pre-reacted material (1 g) was sealed in a quartz ampoule ($22 \times 25 \times 230$ mm) along with I_2 (~ 50 mg) and was kept in a two-

zone furnace at 800–700 °C with a 10-day holding time. Small crystals of a few millimeters were obtained in the cool zone.

Powder XRD measurements were conducted using a Rigaku Smart Lab diffractometer with Cu K α radiation ($\lambda = 1.5418 \text{ \AA}$). Le-Bail refinement analysis was carried out using Jana2006 [39]. XPS data were collected using a VG Microtech ESCA2000 X-ray photoelectron spectrometer using a monochromatic Al-K α X-ray source with 1486.7 eV energy.

The magnetic susceptibility as function of temperature and magnetic field was measured using the vibrational sample magnetometer of a Quantum Design Physical Properties Measurement System. The sample loaded at room temperature was cooled to a low temperature (2 K) without applying magnetic field (zero field cooling, ZFC). At 2 K, a field of 0.1 T was applied, and the susceptibility was measured on heating up to 300 K. The same magnetic field was applied during the second cooling process (field cooling, FC) and data were collected while heating to 300 K. The magnetic moment versus field measurements were conducted at 2 K in the fields range from -14 to 14 T and vice versa.

The room temperature and temperature dependent Raman spectra were collected using Horiba iHR 550 spectrometer with 514 nm wavelength laser and optical setup of own construction with the 532 nm wavelength laser in the inverted mode [40], respectively. The Montana system (Cryostation s50) was used to provide low temperatures in the range between 20 and 250 K. The sample was illuminated by low laser power ($\sim 500 \mu\text{W}$) to protect it from unintentional laser effects and the Raman spectra were collected in reflected geometry. To acquire the Raman spectra, the collected signals were guided to a 50-cm-long spectrometer equipped with a cooled charge-coupled device (CCD) using an optical fiber with a core diameter of 150 μm .

The neutron powder-diffraction (NPD) measurements in the temperature range of 25–300 K were performed using the DN-12 diffractometer (IBR-2 pulsed reactor, JINR, Russia) [41]. The NPD patterns were collected at scattering angle of $2\theta = 90^\circ$ with a resolution of $\Delta d/d = 0.015$. The typical data-collection time for each temperature was 12 h. The experimental data were analyzed by the Rietveld method using the FullProf program [42].

III. RESULTS AND DISCUSSION

A. Crystal structure, chemical composition, and macroscopic magnetic properties

Figure 1(a) depicts the room-temperature XRD patterns of CrPSe₃. The data refinement indicates that the crystal structure of the synthesized CrPSe₃ material belongs to the $C2/m$ space group. No signatures for additional impurity phases in our synthesized CrPSe₃ sample were found. It is worth noting that the structure of monolayer CrPSe₃ is distinctive from other isostructural members of the MPX₃ family with the $C2/m$ space group. Figure 1(b) shows the top (along the z -direction or c^*) and side (along the y -direction or b^*) views. In the monolayer structures of the MPX₃ members ($M = \text{Cr, Mn, Fe, Co, and Ni}$; $X = \text{S, Se}$), metal atoms are located in a honeycomb lattice, and P-P bonds are almost perpendicular to the metal plane. In contrast, the P-P bond of CrPSe₃ was tilted ($\sim 14.5^\circ$) in the direction perpendicular to the Cr plane (Table II). Furthermore, the significant difference in the M-M, P-Se₁, and P-Se₂ bond lengths (denoted in Fig. 1(c) and Table II) creates the C_{2h} point group in monolayer CrPSe₃ instead of the D_{3h} of other MPX₃ [34,43].

The chemical bonding characteristics of CrPSe₃ were investigated by a high-resolution XPS spectroscopy measurements performed for each atom (Fig. 1(d)) - Cr $3p$ (top), P $2p$ (middle), and Se $3d$ (bottom). Deconvolution analysis of the bonding modes revealed the main peaks at 574.41 eV (Cr $2p_{3/2}$) and 585.13 eV (Cr $2p_{1/2}$). In addition, small shadow peaks developed at 575.79 eV

and 583.85 eV imply a presence of weak nonstoichiometry in the studied material. Similarly, shadow peaks were also observed in the XPS spectrum of P-2*p* at 132.45 eV and Se-3*d* at 55.85 eV in addition to the main peaks (e.g., P 2*p*_{3/2} (130.40 eV) and P 2*p*_{1/2} (131.37 eV); Se 3*d*_{5/2} (53.32 eV) and Se 3*d*_{3/2} (54.82 eV)). Quantitative analysis results in the composition of Cr_{0.9}P_{1.1}Se₃, instead of ideal Cr₁P₁Se₃.

We further investigated the magnetic properties of CrPSe₃. Magnetic susceptibility measurements (χ) revealed a magnetization drop below 150 K, indicating the formation of an antiferromagnetic order (Fig. 2(a)). The Néel temperature $T_N \approx 126$ K was extracted from the analysis of the $d\chi/dT$ derivative. The Curie-Weiss temperature (θ_{CW}) and effective magnetic moment (μ_{eff}) were determined from the inverse susceptibility $1/\chi - T$ plot in the 200–250 K range (Fig. 2(b)). The obtained value of $\theta_{CW} \sim -371$ K is the largest one among the members of the MPX₃ family (Table I). It implies a presence of strong short-range antiferromagnetic interactions in CrPSe₃ in the paramagnetic region. The effective magnetic moment of CrPSe₃, $\mu_{eff} \sim 4.6 \mu_B$, corresponds to the high-spin state ($S = 2$) of Cr²⁺ ions. In addition, magnetic field dependent magnetization isotherms (Fig. 2(c)) were measured at 2 K in fields range up to 14 T. The non-linear behavior beyond ± 10 T could be attributed to spin-flop effects at high fields, similar to that found in α -RuCl₃ [44].

The Raman measurements were conducted on exfoliated flakes of CrPSe₃ on a SiO₂/Si substrate obtained by the scotch-tape method. At room-temperature, eight vibrational modes were detected in the 100-350 cm⁻¹ range (Fig. 3(a)). The origin of observed modes is likely associated with the normal modes of the [P₂Se₆]⁴⁺ dimers, which are similar to those of FePS₃ and FePSe₃ [36,43,45,46]. Six Raman vibrational modes were observed in FePS₃ at room temperature in the higher frequency region above 100 cm⁻¹. Nevertheless, more Raman peaks appear in CrPSe₃

since the point group symmetry order is lower in CrPSe₃ compared to that in FePS₃. The number of peaks is unchanged in the temperature-dependent Raman spectra from 20 K to 225 K (Fig. 3(b)), denoting the stability of the monoclinic phase in CrPSe₃ and the absence of the spin-order induced vibrational modes. This is contrasted to the appearance of extra Raman peaks below T_N in FePS₃ [36,45,47]. Nevertheless, anomalous temperature-dependent shift of the vibrational peak located at $\sim 208 \text{ cm}^{-1}$ (assigned as P₆) was clearly revealed (Fig. 3(c)). This peak is associated with the A_{1g} mode of the P₂Se₆ group (inset of Fig. 3(c)) of MPX₃ family, involving partially the Cr-Cr atoms vibrations due to the lower point group symmetry of CrPSe₃. A change of the curve slope in the vicinity of $T_N = 126 \text{ K}$ implies a presence of pronounced spin-phonon coupling, which was also previously found in vdW magnets like CrBr₃ and Cr₂Ge₂Te₆ [20,48]. We did not analyze other detected Raman lines in detail because of their lower intensities.

B. Long range magnetic order and generation of spin density wave

To investigate temperature evolution of the crystal and magnetic structure of CrPSe₃, the neutron powder diffraction (NPD) patterns were measured on cooling to 25 K, as shown in Fig. 4a. The Rietveld refinements of the experimental data revealed that monoclinic symmetry of the crystal structure remains unchanged at low temperatures, in consistence with Raman spectroscopy results (Fig. 4(b)). Below 120 K, appearance of two magnetic peaks at $d_{hkl} = 6.62$ and 7.63 \AA was observed. From the Rietveld analysis of the NPD pattern at 25 K, we found that these peaks are associated with formation of the long-range incommensurate spin density wave (SDW) antiferromagnetic order with the propagation vector $\mathbf{k} = (0, 0.40, 0)$, which can be considered as the modulated zigzag type (Fig. 4(b)). Furthermore, the orientation of the ordered magnetic moments of Cr in the SDW chain is perpendicular to ab plane (Fig. 4(c)). Their values at $T = 25 \text{ K}$, $\mu_{\text{eff}} = 3.2 \mu_B$, are close to those expected for the high-spin state of Cr²⁺ ions. A reduction in the

local ordered magnetic moment compared to effective paramagnetic moment is typical for 2D vdW magnetic materials [18,49–51] and may be related to local magnetic disorder caused by low dimensionality effects.

Compared to other previously known magnetic orders of MPX_3 ($M = \text{Fe, Mn, Ni, X = S, Se}$) systems, which are listed in Table II, CrPSe_3 becomes the unique one with the SDW spin arrangement. To understand the nature of the SDW state in CrPSe_3 , the parameter $f = |\theta_{\text{CW}}|/T_N$, which represents the degree of magnetic frustration, was considered. Typically, values $f > 5$ correspond to strongly frustrated systems with a suppressed long-range magnetic order [52]. The lower values $f \sim 3\text{-}4$ correspond to weakly frustrated systems, where several competitive magnetic orders could be developed, like $\lambda\text{-MnO}_2$ ($f = 3.2$) [53] and TbMnO_3 ($f = 4.2$) [54]. The CrPSe_3 has f value of 2.9, the largest one in the MPX_3 family (Table I). This value is in the range of other weakly frustrated systems such as $\lambda\text{-MnO}_2$ and TbMnO_3 (TbMnO_3 has several transitions, and we consider the lowest transition temperature (~ 10 K) instead of using those of the first incommensurate transition (~ 37 K)). One of the recently proposed scenarios of the SDW state formation in these weakly frustrated systems points to the superposition of two magnetic sets of opposite chirality [51], and it may be also applicable for the present case of CrPSe_3 .

In conclusion, we successfully synthesized CrPSe_3 material by chemical vapor transport method. We found that CrPSe_3 is a weakly frustrated antiferromagnet with the frustration parameter $f \sim 3$, giving rise to formation of the long-range incommensurate spin-density wave state. Our finding is the first report for a weakly frustrated two-dimensional van der Waals insulator, enriching the physics of magnetism at the 2D limit.

ACKNOWLEDGEMENTS

This study was supported by the Institute for Basic Science (Grant number IBS-R011-D1) and Advanced Facility Center for Quantum Technology. Tuan Anh Tran acknowledged for the Vietnam Ministry of Education and Training grant No. B2022-SPK-07.

AUTHOR CONTRIBUTIONS

M. B., N. T. D., and T. A. T. contributed equally to this work.

References:

- [1] H. Kurebayashi, J. H. Garcia, S. Khan, J. Sinova, and S. Roche, *Magnetism, Symmetry and Spin Transport in van Der Waals Layered Systems*, Nat. Rev. Phys. **4**, 150 (2022).
- [2] S. Fukami, C. Zhang, S. Duttagupta, A. Kurenkov, and H. Ohno, *Magnetization Switching by Spin-Orbit Torque in an Antiferromagnet-Ferromagnet Bilayer System*, Nat. Mater. **15**, 535 (2016).
- [3] K. S. Burch, D. Mandrus, and J.-G. Park, *Magnetism in Two-Dimensional van Der Waals Materials*, Nature **563**, 47 (2018).
- [4] C. Gong and X. Zhang, *Two-Dimensional Magnetic Crystals and Emergent Heterostructure Devices*, Science (80-.). **363**, (2019).
- [5] M. Hossain, B. Qin, B. Li, and X. Duan, *Synthesis, Characterization, Properties and Applications of Two-Dimensional Magnetic Materials*, Nano Today **42**, 101338 (2022).
- [6] K. F. Mak, J. Shan, and D. C. Ralph, *Probing and Controlling Magnetic States in 2D Layered Magnetic Materials*, Nat. Rev. Phys. **1**, 646 (2019).
- [7] M. J. Coak et al., *Tuning Dimensionality in Van-Der-Waals Antiferromagnetic Mott Insulators TMPS₃*, J. Phys. Condens. Matter **32**, 124003 (2020).
- [8] M. J. Coak et al., *Emergent Magnetic Phases in Pressure-Tuned van Der Waals Antiferromagnet*, Phys. Rev. X **11**, 011024 (2021).
- [9] M. Onga, Y. Sugita, T. Ideue, Y. Nakagawa, R. Suzuki, Y. Motome, and Y. Iwasa, *Antiferromagnet–Semiconductor Van Der Waals Heterostructures: Interlayer Interplay of Exciton with Magnetic Ordering*, Nano Lett. **20**, 4625 (2020).
- [10] K. Zollner and J. Fabian, *Proximity Effects in Graphene on Monolayers of Transition-Metal Phosphorus Trichalcogenides MPX₃ (M: Mn, Fe, Ni, Co, and X:S,Se)*, Phys. Rev. B

- 106**, 035137 (2022).
- [11] R. Nitsche and P. Wild, *Crystal Growth of Metal-Phosphorus-Sulfur Compounds by Vapor Transport*, Mater. Res. Bull. **5**, 419 (1970).
- [12] A. Wiedenmann, J. Rossat-Mignod, A. Louisy, R. Brec, and J. Rouxel, *Neutron Diffraction Study of the Layered Compounds MnPSe₃ and FePSe₃*, Solid State Commun. **40**, 1067 (1981).
- [13] K. C. Rule, S. J. Kennedy, D. J. Goossens, A. M. Mulders, and T. J. Hicks, *Contrasting Antiferromagnetic Order between FePS₃ and MnPS₃*, Appl. Phys. A Mater. Sci. Process. **74**, 811 (2002).
- [14] R. Gusmão, Z. Sofer, D. Sedmidubský, Š. Huber, and M. Pumera, *The Role of the Metal Element in Layered Metal Phosphorus Triselenides upon Their Electrochemical Sensing and Energy Applications*, ACS Catal. **7**, 8159 (2017).
- [15] C. Gong et al., *Discovery of Intrinsic Ferromagnetism in Two-Dimensional van Der Waals Crystals*, Nature **546**, 265 (2017).
- [16] B. Huang et al., *Layer-Dependent Ferromagnetism in a van Der Waals Crystal down to the Monolayer Limit*, Nature **546**, 270 (2017).
- [17] J. N. Graham, M. J. Coak, S. Son, E. Suard, J.-G. Park, L. Clark, and A. R. Wildes, *Local Nuclear and Magnetic Order in the Two-Dimensional Spin Glass Mn_{0.5}Fe_{0.5}PS₃*, Phys. Rev. Mater. **4**, 084401 (2020).
- [18] A. Bhutani, J. L. Zuo, R. D. McAuliffe, C. R. Dela Cruz, and D. P. Shoemaker, *Strong Anisotropy in the Mixed Antiferromagnetic System Mn_{1-x}Fe_xPSe₃*, Phys. Rev. Mater. **4**, 34411 (2020).
- [19] T. Masubuchi, H. Hoya, T. Watanabe, Y. Takahashi, S. Ban, N. Ohkubo, K. Takase, and

- Y. Takano, *Phase Diagram, Magnetic Properties and Specific Heat of Mn_{1-x}Fe_xPS₃*, J. Alloys Compd. **460**, 668 (2008).
- [20] D. P. Kozlenko, O. N. Lis, S. E. Kichanov, E. V. Lukin, N. M. Belozeroва, and B. N. Savenko, *Spin-Induced Negative Thermal Expansion and Spin–Phonon Coupling in van Der Waals Material CrBr₃*, Npj Quantum Mater. **6**, 1 (2021).
- [21] H. Deiseroth, K. Aleksandrov, C. Reiner, L. Kienle, and R. K. Kremer, *Fe₃GeTe₂ and Ni₃GeTe₂ – Two New Layered Transition-Metal Compounds: Crystal Structures, HRTEM Investigations, and Magnetic and Electrical Properties*, Eur. J. Inorg. Chem. **2006**, 1561 (2006).
- [22] M. A. Susner, M. Chyasnachyus, M. A. McGuire, P. Ganesh, and P. Maksymovych, *Metal Thio- and Selenophosphates as Multifunctional van Der Waals Layered Materials*, Adv. Mater. **29**, 1 (2017).
- [23] R. Samal, G. Sanyal, B. Chakraborty, and C. S. Rout, *Two-Dimensional Transition Metal Phosphorous Trichalcogenides (MPX₃): A Review on Emerging Trends, Current State and Future Perspectives*, Journal of Materials Chemistry A.
- [24] F. Wang et al., *New Frontiers on van Der Waals Layered Metal Phosphorous Trichalcogenides*, Adv. Funct. Mater. **28**, 1802151 (2018).
- [25] M. Birowska, P. E. Faria Junior, J. Fabian, and J. Kunstmann, *Large Exciton Binding Energies in MnPS₃ as a Case Study of a van Der Waals Layered Magnet*, Phys. Rev. B **103**, L121108 (2021).
- [26] S. Kang et al., *Coherent Many-Body Exciton in van Der Waals Antiferromagnet NiPS₃*, Nature **583**, 785 (2020).
- [27] Y. Wang et al., *Emergent Superconductivity in an Iron-Based Honeycomb Lattice*

- Initiated by Pressure-Driven Spin-Crossover*, Nat. Commun. **9**, 1914 (2018).
- [28] P. A. Joy and S. Vasudevan, *Magnetism in the Layered Transition-Metal Thiophosphates MPS_3 ($M = Mn, Fe, \text{ and } Ni$)*, Phys. Rev. B **46**, 5425 (1992).
- [29] G. Le Flem, R. Brec, G. Ouvard, A. Louisy, and P. Segransan, *Magnetic Interactions in the Layer Compounds MPX_3 ($M = Mn, Fe, Ni; X = S, Se$)*, J. Phys. Chem. Solids **43**, 455 (1982).
- [30] A. R. Wildes, B. Roessli, B. Lebech, and K. W. Godfrey, *Spin Waves and the Critical Behaviour of the Magnetization in $MnPS_3$* , J. Phys. Condens. Matter **10**, 6417 (1998).
- [31] K. C. Rule, G. J. McIntyre, S. J. Kennedy, and T. J. Hicks, *Single-Crystal and Powder Neutron Diffraction Experiments on $FePS_3$: Search for the Magnetic Structure*, Phys. Rev. B - Condens. Matter Mater. Phys. **76**, 1 (2007).
- [32] N. Chandrasekharan and S. Vasudevan, *Magnetism and Exchange in the Layered Antiferromagnet $NiPS_3$* , J. Phys. Condens. Matter **6**, 4569 (1994).
- [33] D. Lançon, R. A. Ewings, T. Guidi, F. Formisano, and A. R. Wildes, *Magnetic Exchange Parameters and Anisotropy of the Quasi-Two-Dimensional Antiferromagnet $NiPS_3$* , Phys. Rev. B **98**, 1 (2018).
- [34] K. Kim, S. Y. Lim, J. U. Lee, S. Lee, T. Y. Kim, K. Park, G. S. Jeon, C. H. Park, J. G. Park, and H. Cheong, *Suppression of Magnetic Ordering in XXZ -Type Antiferromagnetic Monolayer $NiPS_3$* , Nat. Commun. **10**, (2019).
- [35] Y. Shemerliuk, Y. Zhou, Z. Yang, G. Cao, A. U. B. Wolter, B. Büchner, and S. Aswartham, *Tuning Magnetic and Transport Properties in Quasi-2D $(Mn_{1-x}Ni_x)_2P_2S_6$ Single Crystals*, Electron. Mater. **2**, 284 (2021).
- [36] J.-U. Lee, S. Lee, J. H. Ryoo, S. Kang, T. Y. Kim, P. Kim, C.-H. Park, J.-G. Park, and H.

- Cheong, *Ising-Type Magnetic Ordering in Atomically Thin FePS₃*, Nano Lett. **16**, 7433 (2016).
- [37] D. Lançon, H. C. Walker, E. Ressouche, B. Ouladdiaf, K. C. Rule, G. J. McIntyre, T. J. Hicks, H. M. Rønnow, and A. R. Wildes, *Magnetic Structure and Magnon Dynamics of the Quasi-Two-Dimensional Antiferromagnet FePS₃*, Phys. Rev. B **94**, 214407 (2016).
- [38] N. Chandrasekharan and S. Vasudevan, *Magnetism, Exchange and Crystal Field Parameters in the Orbitally Unquenched Ising Antiferromagnet FePS₃*, Pramana **43**, 21 (1994).
- [39] V. Petříček, M. Dušek, and L. Palatinus, *Crystallographic Computing System JANA2006: General Features*, Zeitschrift Für Krist. - Cryst. Mater. **229**, 345 (2014).
- [40] K. P. Dhakal, D. L. Duong, J. Lee, H. Nam, M. Kim, M. Kan, Y. H. Lee, and J. Kim, *Confocal Absorption Spectral Imaging of MoS₂: Optical Transitions Depending on the Atomic Thickness of Intrinsic and Chemically Doped MoS₂*, Nanoscale **6**, 13028 (2014).
- [41] V. L. Aksenov et al., *DN-12 Time-of-Flight High-Pressure Neutron Spectrometer for Investigation of Microsamples*, Phys. B **265**, 258 (1999).
- [42] J. Rodríguez-Carvajal, *Recent Advances in Magnetic Structure Determination by Neutron Powder Diffraction*, Phys. B **192**, 55 (1993).
- [43] M. Bernasconi, G. L. Marra, G. Benedek, L. Miglio, M. Jouanne, C. Julien, M. Scagliotti, and M. Balkanski, *Lattice Dynamics of Layered MPX₃ (M=Mn,Fe,Ni,Zn; X=S,Se) Compounds*, Phys. Rev. B **38**, 12089 (1988).
- [44] J. A. Sears, M. Songvilay, K. W. Plumb, J. P. Clancy, Y. Qiu, Y. Zhao, D. Parshall, and Y.-J. Kim, *Magnetic Order in α -RuCl₃: A Honeycomb-Lattice Quantum Magnet with Strong Spin-Orbit Coupling*, Phys. Rev. B **91**, 144420 (2015).

- [45] M. Scagliotti, M. Jouanne, M. Balkanski, G. Ouvrard, and G. Benedek, *Raman Scattering in Antiferromagnetic FePS₃ and FePSe₃ Crystals*, Phys. Rev. B **35**, 7097 (1987).
- [46] M. L. Sanjuán, M. A. Kanehisa, and M. Jouanne, *Electronic Raman Study of Fe²⁺ in FePX₃(X=S,Se) Layered Compounds*, Phys. Rev. B **46**, 11501 (1992).
- [47] M. Scagliotti, M. Jouanne, M. Balkanski, and G. Ouvrard, *Spin Dependent Phonon Raman Scattering in Antiferromagnetic FePS₃ Layer-Type Compound*, Solid State Commun. **54**, 291 (1985).
- [48] Y. Tian, M. J. Gray, H. Ji, R. J. Cava, and K. S. Burch, *Magneto-Elastic Coupling in a Potential Ferromagnetic 2D Atomic Crystal*, 2D Mater. **3**, (2016).
- [49] D. Lançon, H. C. Walker, E. Ressouche, B. Ouladdiaf, K. C. Rule, G. J. McIntyre, T. J. Hicks, H. M. Rønnow, and A. R. Wildes, *Magnetic Structure and Magnon Dynamics of the Quasi-Two-Dimensional Antiferromagnet FePS₃*, Phys. Rev. B **94**, 214407 (2016).
- [50] A. R. Wildes, V. Simonet, E. Ressouche, R. Ballou, and G. J. McIntyre, *The Magnetic Properties and Structure of the Quasi-Two-Dimensional Antiferromagnet CoPS₃*, J. Phys. Condens. Matter **29**, 455801 (2017).
- [51] A. R. Wildes, K. C. Rule, R. I. Bewley, M. Enderle, and T. J. Hicks, *The Magnon Dynamics and Spin Exchange Parameters of FePS₃*, J. Phys. Condens. Matter **24**, 416004 (2012).
- [52] L. Balents, *Spin Liquids in Frustrated Magnets*, Nature **464**, 199 (2010).
- [53] J. E. Greedan, N. P. Raju, A. S. Wills, C. Morin, S. M. Shaw, and J. N. Reimers, *Structure and Magnetism in λ -MnO₂. Geometric Frustration in a Defect Spinel*, Chem. Mater. **10**, 3058 (1998).
- [54] M. Staruch, D. Violette, and M. Jain, *Structural and Magnetic Properties of Multiferroic*

- Bulk TbMnO₃*, Mater. Chem. Phys. **139**, 897 (2013).
- [55] A. Jain et al., *Commentary: The Materials Project: A Materials Genome Approach to Accelerating Materials Innovation*, APL Mater. **1**, 011002 (2013).
- [56] R. Brec, *Review on Structural and Chemical Properties of Transition Metal Phosphorous Trisulfides MPS₃*, in (1986), pp. 93–124.
- [57] A. R. Wildes et al., *Magnetic Structure of the Quasi-Two-Dimensional Antiferromagnet NiPS₃*, Phys. Rev. B **92**, 224408 (2015).
- [58] C. C. Mayorga-Martinez, Z. Sofer, D. Sedmidubský, Š. Huber, A. Y. S. Eng, and M. Pumera, *Layered Metal Thiophosphite Materials: Magnetic, Electrochemical, and Electronic Properties*, ACS Appl. Mater. Interfaces **9**, 12563 (2017).
- [59] K. Kurosawa, S. Saito, and Y. Yamaguchi, *Neutron Diffraction Study on MnPS₃ and FePS₃*, J. Phys. Soc. Japan **52**, 3919 (1983).
- [60] E. Ressouche, M. Loire, V. Simonet, R. Ballou, A. Stunault, and A. Wildes, *Magnetolectric MnPS₃ as a Candidate for Ferrotoroidicity*, Phys. Rev. B - Condens. Matter Mater. Phys. **82**, 1 (2010).
- [61] R. Brec, *Review on Structural and Chemical Properties of Transition Metal Phosphorous Trisulfides MPS₃*, Solid State Ionics **22**, 3 (1986).

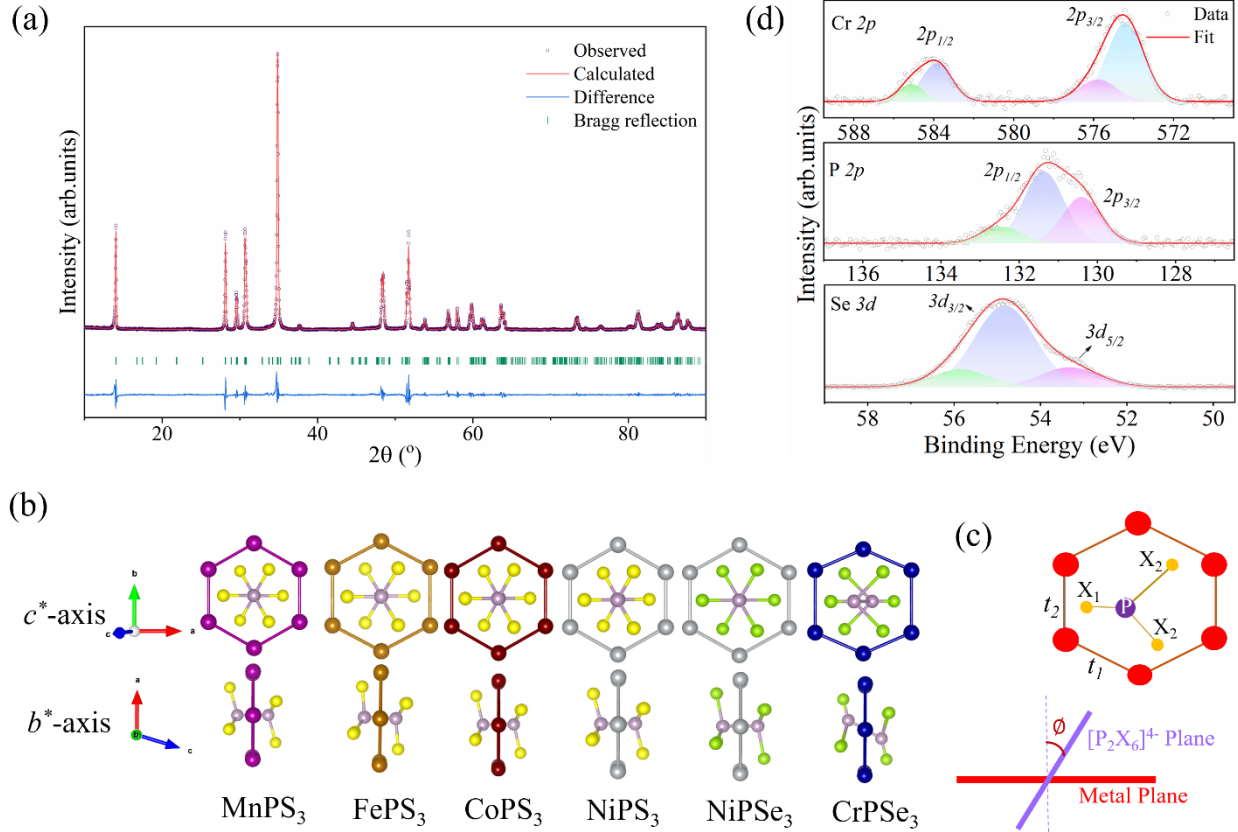


FIG. 1. (a) Room temperature x-ray diffraction pattern of the synthesized CrPSe₃ material. The experimental points, calculated profile, Bragg reflections positions and difference curve are shown. (b) Monolayer structure comparison among members of MPX₃ (M = Cr, Mn, Fe, Co, and Ni; X = S, Se) family. The metal atoms are located in a honeycomb lattice and ([P₂Se₆]⁴⁻) dimer is located in a perpendicular plane to metal plane. (c) The layout of the M-M distances (t_1 , t_2) in honeycomb lattice, the P-P, and P-X distances, which values are listed in Table II. (d) High-resolution x-ray photoelectron spectra and peak deconvolution of Cr 2*p*, P 2*p*, and Se 3*d*.

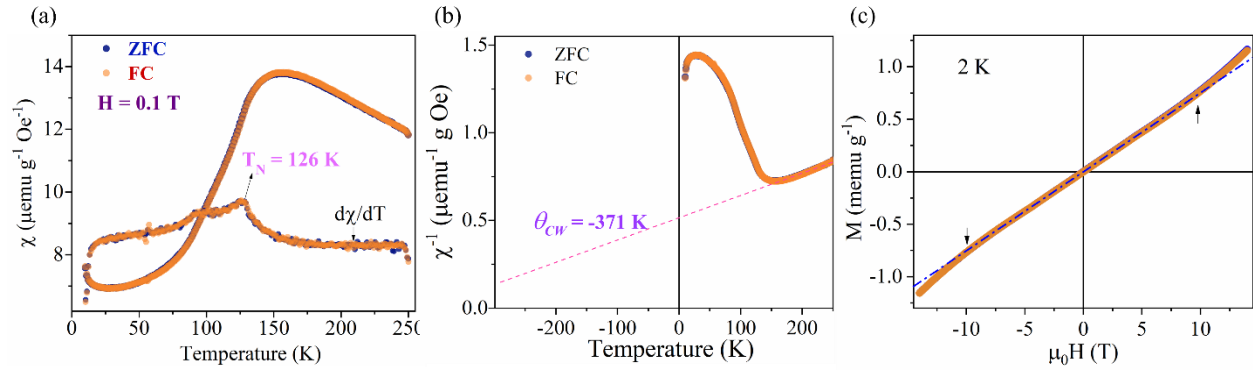


FIG. 2. (a) Magnetic susceptibility of CrPSe₃ powder as a function of temperature measured at $H = 1 \text{ kOe}$, the $\chi - T$ curves, blue color for zero field cooling (ZFC) and orange color for field cooling (FC), showing antiferromagnetic transition with the Néel temperature $T_N \sim 126 \text{ K}$ (extracted from the $d\chi/dT$ versus T curve). (b) χ^{-1} versus T curve, high Curie-Weiss temperature indicates strong exchange interactions in paramagnetic region (above T_N). (c) Field dependent magnetization measured at 2 K .

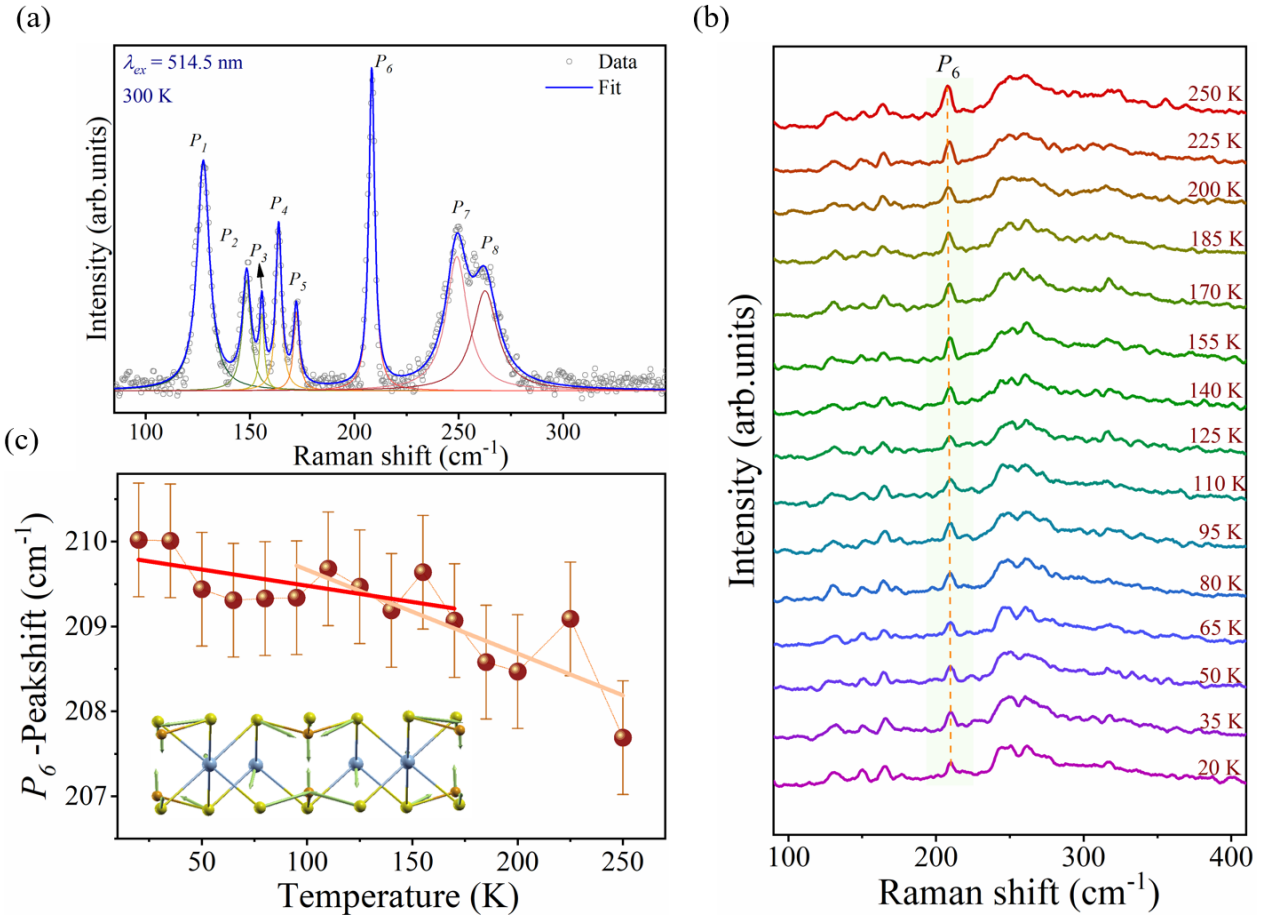


FIG. 3. (a) Raman spectra of CrPSe₃ showing prominent vibrational modes at room temperature, (b) Temperature-dependent Raman spectra at 20–250 K indicate unchanged crystal structure throughout the temperature region as indicated by the consistent vibrational modes. (c) The evolution of the P₆ peak with temperature, revealing two different slopes at a critical temperature of 125 K.

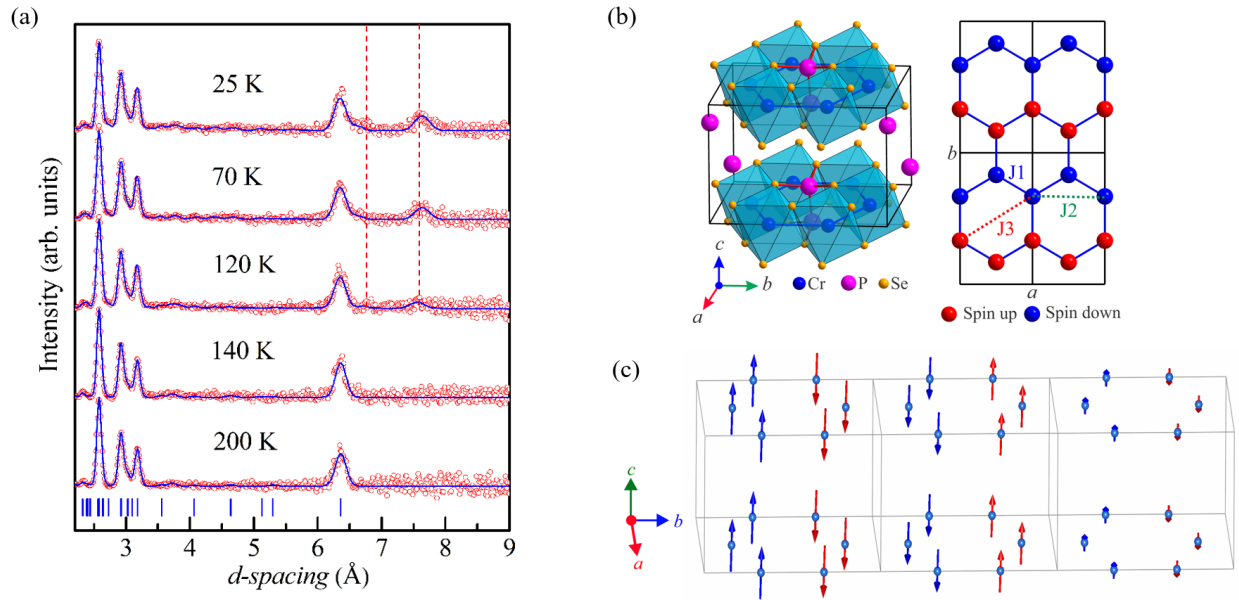


FIG. 4. (a) The powder neutron diffraction patterns measured from 25 K to 200 K. The experimental points, calculated profiles and calculated nuclear peaks positions are shown. The appearance of additional magnetic peaks at 6.7 Å and 7.5 Å below 140 K indicates the formation of antiferromagnetic order consistent with magnetic susceptibility. (b) The monoclinic crystal structure extracted from Rietveld refined data (*left*) and spin configuration (*right*), J_1 , J_2 , and J_3 are exchange interaction energies of first, second, third nearest neighbors, respectively. (c) The incommensurate spin density wave magnetic structure formed in CrPSe₃. The values of the ordered magnetic moments vary along the b-axis.

TABLE I. Crystal structure, antiferromagnetic transition temperatures, effective paramagnetic and ordered magnetic moments, types of magnetic order, and in-plane exchange energies of MPX_3 family of materials in comparison with $CrPSe_3$.

Compound	Crystal Structure (Space group)	Spin order	T_N (K)	θ_{CW} (K)	$f = \frac{ \theta_{CW} }{T_N}$	$\mu_{eff} (\mu_B)$	
						$\chi(T)-T$	NPD
NiPSe ₃ [29,55]	Monoclinic (C2/m)	zigzag	206	-	-	-	-
NiPS ₃ [28,33,35]	Monoclinic (C2/m)	zigzag	155	-254	~1.6	3.9 [56]	1.06 [57]
CoPS ₃ [50,58]	Monoclinic (C2/m)	zigzag	122,132	-116, -223	0.9,1.9	4.9 [50]	4.9 [56]
FePSe ₃ [12,18]	Rhombohedral (R-3)	zigzag	112	-9	~0.1	5.2 [18]	4.2 [18]
FePS ₃ [13,28]	Monoclinic (C2/m)	zigzag	118,119	-112	~1.0	4.9 [56]	4.5 [49]
MnPSe ₃ [12,18]	Rhombohedral (R-3)	Néel	74	-146	~2.0	5.9 [18]	3.6 [18]
MnPS ₃ [13,19,28]	Monoclinic (C2/m)	Néel	78,80	-160	~2.0	5.98 [56]	4.1 [59]
CrPSe₃ [This work]	Monoclinic (C2/m)	zigzag	126	-371	2.9	4.6	3.2

TABLE II. The structural parameters characterizing monolayer geometry among members of the MPX_3 family compared to $CrPSe_3$, including lattice parameters, M-M distance on hexagonal lattice (t_1 and t_2 shown in Fig. 1(c)), P-P, P-X distance, $[P_2X_6]^{4-}$ dimer deviation angle from a perpendicular to metal plane (\emptyset).

Compound	Lattice parameters		M-M distance	Bond lengths (P-P & P-X)	Deviation (\emptyset)
MnPS ₃ [60]	$a = 6.0770 \text{ \AA}$ $b = 10.5240 \text{ \AA}$ $c = 6.7960 \text{ \AA}$	$\alpha = \gamma = 90^\circ$, $\beta = 107.3500^\circ$ $V = 414.8583 \text{ \AA}^3$	$t_1 = 3.5005 \text{ \AA}$ $t_2 = 3.5239 \text{ \AA}$	$d_{P-P} = 2.1874 \text{ \AA}$ $d_{P-S1} = 2.0342 \text{ \AA}$ $d_{P-S2} = 2.0296 \text{ \AA}$	0.119°
FePS ₃ [49]	$a = 5.9400 \text{ \AA}$ $b = 10.2600 \text{ \AA}$ $c = 13.2000 \text{ \AA}$	$\alpha = \gamma = 90^\circ$, $\beta = 108.3000^\circ$ $V = 763.7806 \text{ \AA}^3$	$t_1 = 3.3641 \text{ \AA}$ $t_2 = 3.5500 \text{ \AA}$	$d_{P-P} = 2.0566 \text{ \AA}$ $d_{P-S1} = 2.0318 \text{ \AA}$ $d_{P-S2} = 2.0744 \text{ \AA}$	2.058°
CoPS ₃ [37]	$a = 5.9010 \text{ \AA}$ $b = 10.2220 \text{ \AA}$ $c = 6.6580 \text{ \AA}$	$\alpha = \gamma = 90^\circ$, $\beta = 107.1700^\circ$ $V = 383.7122 \text{ \AA}^3$	$t_1 = 3.3874 \text{ \AA}$ $t_2 = 3.4469 \text{ \AA}$	$d_{P-P} = 2.1501 \text{ \AA}$ $d_{P-S1} = 2.0392 \text{ \AA}$ $d_{P-S2} = 2.0556 \text{ \AA}$	0.223°
NiPS ₃ [61]	$a = 5.8120 \text{ \AA}$ $b = 10.0700 \text{ \AA}$ $c = 6.6320 \text{ \AA}$	$\alpha = \gamma = 90^\circ$, $\beta = 106.9800^\circ$ $V = 371.2293 \text{ \AA}^3$	$t_1 = 3.3525 \text{ \AA}$ $t_2 = 3.3634 \text{ \AA}$	$d_{P-P} = 2.1693 \text{ \AA}$ $d_{P-S1} = 1.9851 \text{ \AA}$ $d_{P-S2} = 1.9890 \text{ \AA}$	0.005°
NiPSe ₃ [55]	$a = 6.1604 \text{ \AA}$ $b = 10.6768 \text{ \AA}$ $c = 6.9323 \text{ \AA}$	$\alpha = \gamma = 90^\circ$, $\beta = 107.1791^\circ$ $V = 435.6165 \text{ \AA}^3$	$t_1 = 3.5574 \text{ \AA}$ $t_2 = 3.5586 \text{ \AA}$	$d_{P-P} = 2.2413 \text{ \AA}$ $d_{P-Se1} = 2.2466 \text{ \AA}$ $d_{P-Se2} = 2.2468 \text{ \AA}$	0.055°
CrPSe₃ [This work]	$a = 6.1246 \text{ \AA}$ $b = 10.6705 \text{ \AA}$ $c = 6.6950 \text{ \AA}$	$\alpha = \gamma = 90^\circ$, $\beta = 107.8560^\circ$ $V = 416.4593 \text{ \AA}^3$	$t_1 = 3.3428 \text{ \AA}$ $t_2 = 3.9948 \text{ \AA}$	$d_{P-P} = 2.2255 \text{ \AA}$ $d_{P-Se1} = 2.0307 \text{ \AA}$ $d_{P-Se2} = 2.2995 \text{ \AA}$	14.472°